Microscopic Mechanisms of Sonoporation

P.A. Prentice[1,2], J.M. Burns[1], A. Cuschieri[1] and P. A. Campbell[1,2]

[1]Department of Surgery and Molecular Oncology, Ninewells Hospital,
University of Dundee, Dundee DD1 9SY, Scotland, UK.
[2]Faculty of Engineering & Physics, University of Dundee, Dundee DD1 4HN, Scotland.

ABSTRACT

Achieving remote and non-invasive molecular delivery to cells is an area of increasing industrial and academic interest. A focus for current research activity involves ultrasound exposure (insonation) in the presence of contrast agent microbubbles, which is known to enhance membrane permeability and lead to molecular uptake from the locale[1]. Under high ultrasound pressures (>0.2MPa), this process (sonoporation) can elicit a number of clinically relevant bioeffects such as direct lysis [1,2] and apoptosis [2-4]. Moreover, promising observations of tumour regression have been demonstrated in murine studies [5,6]. However, whilst speculation regarding the physical mechanisms responsible for membrane permeabilization has been widespread, corroboration has, until very recently [7,8] remained elusive. Here we present further direct observational evidence that illuminates the dynamical processes relating to individual cavitation events near cells and which, we speculate, provides a cogent explanation for previous statistical studies on insonated cell populations using flow cytometry .

Keywords: sonoporation, cavitation, microbubbles, ultrasound, optical trapping.

1 INTRODUCTION

Ultrasonic approaches to therapy are attractive as they have potential for undertaking specific surgical interventions without the need for a physical incision. The process of permeabilizing a cell membrane via exposure to ultrasound is known as sonoporation. The principal experimental arrangement employed for sonoporation studies thus far have employed fluid suspensions of cells within cuvettes [1-4,6]. Subsequent statistical analyses on insonated populations based on flow cytometry [2-4, 9] and hemocytometry [1,10] measurements have demonstrated that uptake levels can be accurately quantified (see Figure 1). Moreover, distinct bioeffects have also been discriminated. Whilst such experiments do not by themselves allow for a categorical identification of uptake mechanism, they at least define numerical limits, in terms of the number of molecules taken up from the ambient fluid, within which mechanistic explanations must be consistent. Similarly, when electron-microscope based characterisations of native (control) and insonated cell membranes are compared, evidence for localised penetrating events has arisen [11,12]. However, in order to draw definitive conclusions on the mechanistic possibilities for permeabilization, and thus consolidate the inferences from previous indirect observations, we require confirmation by direct imaging of the actual precursor events that disrupt the membrane followed by correlation with any induced membrane features. Our experiments have realised both these critical objectives. Moreover, direct comparison of the distinct modes of permeabilization that we have observed, with previous reports measuring uptake levels in sonoporation via flow cytometry and fluorescent microscopy (viz Fig. 1), facilitates a coherent description of the sub-classes of populations that often arise during such statistical analyses of sonoporated cells.

We begin by describing the novel apparatus that has been developed specifically for this research project.

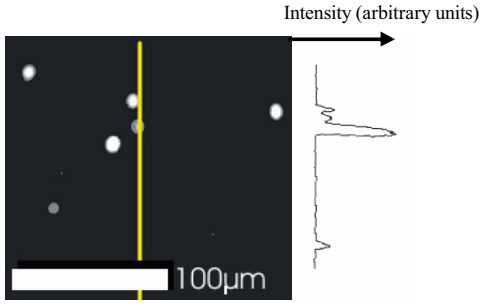

Figure 1. Fluorescence microscopy on post-insonated cells. During exposure, the cells had been suspended in physiological buffer in an ultrasound transparent cuvette also containing fluorescent calcein to indicate the extent of uptake. After washing and deposition onto a coverslip for qualitative fluorescence microscopy we typically found three levels of uptake: high (bright), low (intermediate brightness), and nominal (dark). The plot (RHS) shows an optical intensity cross-section (arbitrary units) corresponding to the yellow line in the main figure.

2. APPARATUS & METHODS

In order to converge on the imaging objectives stated above, it was crucial that our experimental design (Figure 2) facilitated direct observation without geometric constraint or interference to the natural hydrodynamic

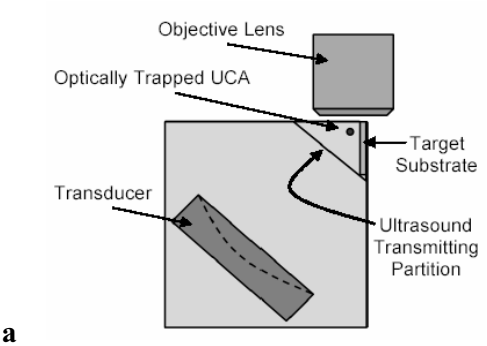

Figure 2(a). Schematic view of the optical-trapping/insonation chamber architecture (not to scale). The focus of the ultrasound transducer is precalibrated using a hydrophone and the coverslip substrate is located within this region. The x60 objective lens serves as both the focus element for the Laguerre-Gaussian vortex beam and also the chief magnification objective to the Imacon high speed system. (b) 2D intensity profile of the Laguerre-Gauss beam. A hollow microbubble can be readily trapped in the core (c), and transported (d), to a well defined displacement from a substrate.

environment in the vicinity of the cavitating ultrasound-contrast agent (UCA). This was achieved by hybridizing optical trapping [13] (OT) [to spatially control individual UCA relative to a substrate], together with ultra-high speed (UHS) imaging to monitor the cavitation dynamics. The UCA employed (Optison) consist of denatured albumin shells surrounding gas [octafluoropropane] cores, with diameters ranging from 2-7μm. Hollow UCA exhibit a lower refractive index relative to the surrounding fluid, therefore OT in conventional Gaussian beams is unfeasible. We implemented a Laguerre-Gaussian (LG) profile [14] via a phase modulating static hologram [15] for our diffractive optic element. This maximises intensity (and thus trapping force) and effectively redefined the intrinsic TEM_{00} (l=0) mode emanating from a Nd:YVO_4 solid state laser. This laser was selected specifically as its wavelength (1064 nm) is generally accepted to minimise cytotoxic effects. The hologram effectively redefines the laser profile to a TEM_{01} (l=3) LG mode with intensity distribution orthogonal to the laser axis, $I(r)$, thus:

$$I(r) \propto \exp\left(\frac{-r^2}{\omega_0^2}\right)\tanh\left(\frac{r}{\omega_v}\right) \quad (1)$$

where, ω_0 corresponds to the precursor Gaussian beam width, and ω_v is the characteristic core size selected to accommodate UCA of diameter ~ 5μm [16].

Once trapped, UCA were guided to a controllable **z**-displacement from the coverslip plane (Fig. 2(c-d)), and an insonation protocol applied (typically 20μs burst of 1MHz ultrasound (US) at peak negative pressure (PNP) 1.39MPa (±14%) unless otherwise stated), with synchronous triggering of the UHS data acquisition.

3 RESULTS

Over 600 UHS sequences have been acquired using the combined OT/UHS approach to stabilize UCA relative to substrates prior to insonation. We have previously reported on those observations where obvious contact between the cavitating UCA and underlying cells occurred [8]. We now expand on those initial observations and moreover, suggest a link between the mechanistic possibilities that our own observations support, with the statistical measurements of molecular uptake previously reported in the literature.

3.1 Cell Compression

Coverslips supporting cultured monolayers of adherent live MCF7 (human breast cancer) cells at 70-80% confluence, were introduced to the sonoporation chamber containing Dulbeccos modified Eagle's medium (DMEM), and insonation repeated with optically trapped UCA at normal displacements typically between 1-5 bubble diameters from the membrane plane. When the maximum UCA radius during cavitation just exceeded the initial displacement of the quiescent UCA from the monolayer of cells, then the dominant finding was quasi-spherical expansion with contact, and compression of underlying cells, as illustrated in Figure 3 below.

The induced membrane tension under this circumstance may be sufficient to disrupt the membrane if it exceeds that critical for rupture. Assuming the entire membrane is stretched during this deformation process, and estimating the membrane areal increase ΔA, and its initial area A_0, we can compute the resultant areal strain as ($\Delta A/A_0$). The critical areal strain for a bilipid membrane is routinely quoted as between 2-5% [17,18] and thus a cell may thus be rendered permeable in this process if that range is exceeded. Approximating $A_0 \sim 2(pi)R^2(1-\cos\theta)$, where R is the radius of curvature of the cell, and θ is the angle the cell membrane makes with the coverslip (typically 30°), then ΔA introduced by compression via the inflated UCA shell is given by $(pi)R_S^2$, where R_S is the radius of the spherically-capped compression zone, recognised as the topological deformation of a circular patch of membrane also of radius R_S. Thus for an average cell monolayer at around 85% confluence, membrane breaching can be expected when the following [equivalent] conditions are met:

$$(\Delta A/A_0) \sim piR_S^2/\ 2piR^2(1-\cos\theta) > 0.05 \quad (2a)$$

$$\Rightarrow [R_S^2/\ (2R^2(1-\sqrt{3}/2))] > 0.05 \quad (2b)$$

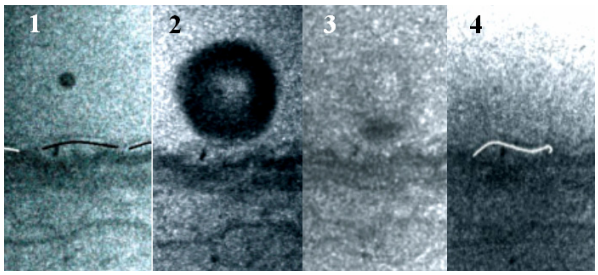

Figure 3. A 5.0μm diameter microbubble trapped to circa 17μm from a cell (membrane outlined) in a monolayer, and exposed to US of PNP: 3.70±1.48 MPa. The microbubble is seen to inflate to maximum radius (frame 2 at t =4.0μs) and into osculation with the membrane, compressing it in the process. Comparison of frames 1 and 4 captured at t<0μs and t=12.0μs respectively reveals the extent of the resulting deformation.

Interestingly, during post insonation interrogation using scanning probe microscopy, even for large compression ratios, we did not observe any membrane breaches from such events. It may be that the pores are unstable and quickly reform to seal the membrane effectively, or that they are so small as to fall below the spatial resolution of the microscope (several 10s of nanometers for the present set-up). Further experiments in real-time systems are clearly required.

3.2 Microjetting

The only occasion when we observed quite definite membrane disruption was after an active microjet event had occurred with a directionality into the plane of the cells monolayers [8]. Here, UCA microbubbles are seen to experience inertial cavitation and collapse, with the outermost hemisphere undergoing involution to form a central reentrant jet directed at the cell (viz Figure 4). Membrane breaching is possible if such jets can induce sufficient stress to exceed the critical rupture stress, t_{max}, that is related to the local elastic modulus E thus:

$$t_{max} = E\varepsilon_r \qquad (3)$$

where ε_r is the relative deformation before rupture, the maximum for which is 2-5% (ε_r=0.02-0.05) in human cells [17,18]. Measurements of E on live cells have produced results consistently below 100kPa [19, 20] leading to an approximate upper limit of t_{max} ~ 2-5kPa.

We have shown previously [8] that either the development of a water hammer pressure *or* momentum exchange due to fluid flow can generate sufficient pressures to exceed this threshold with ease and thus either mode may be a viable microscopic mechanism for permeabilizing cells.

3.3 Scanning Probe Microscopy

In order to examine the penetrability of UCA derived microjets, post-insonation membrane topography was interrogated using atomic force microscopy (AFM). Pits (sonopores) were consistently observed on all cells previously located directly below the hypocentre of trapped UCA that underwent microjetting into cells. Figure 4 shows a typical sonopore formed due to a microjetting event. A cross-section through this entity reveals that it measures approximately 12.5μm across, similar to that observed during UHS imaging of the contact phases of microjet touchdown within this regime of ultrasound intensity. Moreover, the jet penetration power was such that sonopore depth extends to the underlying coverslip. In Figure 4 the perspective AFM image of a representative sonopore exhibits a distinct peripheral lip of raised material: this is another consistent occurrence arising through microjet contact with the membrane.

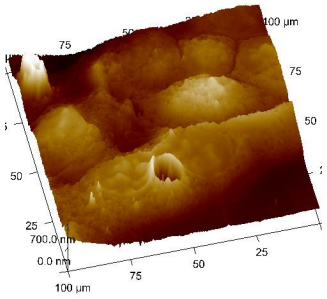

Figure 4. Atomic force microscopy of a sonopore arising via interaction with a cavitation derived microjet.

The spatial extent of these microjet induced sonopores suggests that such events probably lead to cell lysis: indeed, this echoes the findings of others, that insonation in the presence of Optison with elevated US pressures potentiates cell killing [1,2] However, if damage to the nucleus, and vital organelles is avoided, then even large membrane disruptions, up to 1000μm^2, have been shown to reseal [21] and a cell might remain viable after microjet penetration. For application of lower mechanical index ultrasound, we have also seen that much smaller sonopores can form. We note however that even for larger sonopores of the order seen in Figure 4 above, then the actual 'healing time' to reform this damage and reconstruct the internal cytoskeleton is not of the same order as the time required to reseal the membrane along the sonoporation induced wound internally. This latter process appears to occur over the order of seconds [22] and probably involves a relatively fast vesicle patching phenomenon, as suggested in ref. 21, whereas the former process appears to occur over some 10s of minutes, assuming that the cell actually remains viable.

4 CONCLUSIONS

Spatially controlled UHS observations of cavitating UCA microbubbles near cellular interfaces have provided valuable new insights, especially to the dynamic processes that can arise within high pressure insonation regimes. Moreover, calculations support their possible role as permeabilization modes in sonoporation. The mechanistic possibilities are distinct, have differing temporal effects on the affected cells, and exhibit differing statistics [8] depending on the environment. Although it is recognized that microbubble cavitation in the presence of substrates supporting monolayers will be different to that in a cell suspension, we speculate (with the aid of detailed calculations [23]) that the population analyses arising through flow cytometry experiments [see ref 9 for example, as well as the illustration in Figure 5 below and the image in Figure 1] may exhibit their distinct three peak characteristics [nominal, low and high uptakes] due to those specific cell sub populations having undergone respectively (i) negligible interaction with cavitating UCA; (ii) compression breaching (with fast resealing so that short term diffusion driven loading may occur), and (iii) microjetting and microinjection to load the cell maximally.

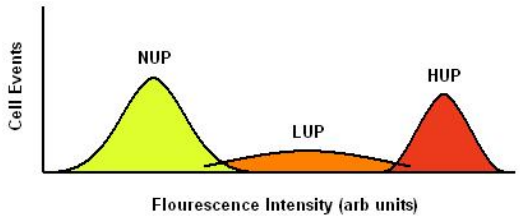

Figure 5. Fluorescent populations from flow cytometry analyses [after the fashion of ref 9] for cells exposed to US in the presence of calcein and Optison. Cells exhibit heterogeneous loading and can be designated as nominal uptake population (NUP) with fluorescence signal only marginally greater than that of control cells; low uptake population (LUP) exhibiting a wide range of uptake levels and finally a high uptake population (HUP).

We anticipate that further combined OT/UHS experiments, especially with parallel fluorescence microscopy, will provide further strong evidence in favour of this suggestion.

Acknowledgements

We thank RCUK and the EPSRC for financial support through grants EP/D048958 and GR/T23688/1 respectively, and also thank SHEFC (now SFC) for an SRDG grant also. We also gratefully acknowledge the EPSRC Instrument Loan Pool at the Rutherford Appleton Laboratory (Peter Anthony and Adrian Walker) for supplying both ultra high speed imaging systems. We are indebted to our ongoing collaborators: Kishan Dholakia and Wilson Sibbett (St Andrews), Mark Prausnitz (Georgia Tech), Michiel Postema (Ruhr-Bochum) for invaluable discussions; and Jean Christophe Bourdon and Pamela Robertson (Dundee) for assistance with the cell culture activities. JMB also acknowledges the EPSRC for a DTA studentship award.

*Address correspondence to: (p.a.campbell@dundee.ac.uk)

REFERENCES

[1] Ward, M., Wu, J. & Chiu, J.F. *J. Acoust. Soc. Amer.* **105,** 2951-2957 (1999)
[2] Feril, L.B. *et al*. *Ultrasound in Med. Biol.* **29,** 331-337 (2003)
[3] Honda, H., Kondo, T., Zhao, Q.L., Feril, L.B. & Kitagawa, H. *Ultrasound in Med. Biol.* **30,** 683-692 (2004)
[4] Honda, H., Zhao, Q.L. & Kondo, T. *Ultrasound in Med. Biol.* **28**, 673-682 (2002)
[5] Miller, D.L. & Song, J. *Ultrasound in Med. Biol.* **29**, 887-893 (2003)
[6] Rapoport, N.Y., Christensen, D.A., Fein, H.D., Barrows, L. & Gao, Z. Ultrasound triggered drug targeting of tumors in vitro and in vivo. *Ultrasonics* **42,** 943-950 (2004)
[7] Marmottant. P & Hilgenfeldt, S. *Nature* **423**, 153-156 (2002)
[8] Prentice PA *et al*. *Nature Physics* **1**, 107-110 (2005)
[9] Guzman, H.R., Nguyen, D.X., Khan, S. & Prausnitz, M.R. *J. Acoust. Soc. Amer.* **110,** 597-606 (2001)
[10] Ward, M., Wu, J. & Chiu, J.F. *Ultrasound in Med. Biol***. 26**, 1169-1175 (2000)
[11] Tachibana, K., Uchida, T.,Ogawa, K.,Yamahita, N. &Tamura, K. *Lancet* **353**, 1409 (1999)
[12] Wang, W., Bian, Z.Z., Wu, Y., Zhou, Q. W., & Miao, Y.L. *J. Ultrasound. Med.* **23**, 1569-1582 (2004)
[13] Ashkin, A., Dziedzic, J.M., Bjorkholm, J.E. & Chu, S. *Optics Letters* **11**, 288 (1986)
[14] Gahagan, K.T. & Swartzlander, G.L. *J. Opt. Soc. Amer. B* **15,** 524-534 (1998)
[15] Swanson, G.J. & Veldkamp, W.B. *Optical Engineering* **28**, 605-608 (1989)
[16] Prentice, P.A. *et al*. *Optics Express* **12,** 593-603 (2004)
[17] Lokhandwalla, M. & Sturtevant, B. *Phys. Med. Biol*. **46,** 413-437 (2001)
[18] Boal, D. *Mechanics of the Cell*. (Cambridge University Press 2002)
[19] Rotch, C., Jacobson, K., & Radmacher, M.. *Proc. Nat. Acad. Sci. USA* **96**, 921-926 (1999)
[20] Campbell, P.A., Cuschieri, A., Liovic, M. & Lane, E.B. *Inst. Physics. Conf. Series.* **168,** 517-520 (2001)
[21] Steinhardt, R.A., Bi, G. & Alderton, J.M.. *Science* **263**, 390-393 (1994)
[22] Deng, C., Seiling F., Pan H., & Cui, J. *Ultrasound Med Biol* 30 519-526 (2004)
[23] Campbell PA & Prentice PA, *to be published*. (2006)